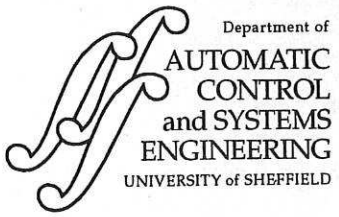

DYNAMIC CHARACTERISATION OF A FLEXIBLE MANIPULATOR SYSTEM

M O Tokhi and Z Mohamed

Department of Automatic Control and Systems Engineering,
The University of Sheffield, Mappin Street, Sheffield, S1 3JD, UK.

Tel: + 44 (0)114 222 5617.
Fax: + 44 (0)114 222 5661.
E-mail: o.tokhi@sheffield.ac.uk.

Research Report No. 798

August 2001

Abstract

This paper presents theoretical and experimental investigations into the dynamic modelling and characterisation of a flexible manipulator system. A constrained planar single-link flexible manipulator is considered. A dynamic model of the system is developed based on finite element methods. The flexural and rigid dynamics of the system as well as inertia effects and structural damping are accounted in the model. Performance of the algorithm in describing the dynamic behaviour of the system is assessed in comparison to an experimental test-rig. Experimental results are presented for validation of the developed finite element model in the time and frequency domains.

Keywords: Dynamic modelling, flexible manipulator, finite element method.

CONTENTS

LIST OF TABLES AND FIGURES

1. Introduction

Most existing robotic manipulators are designed and built in a manner that maximise stiffness, in an attempt to minimise system vibration and achieve good positional accuracy. High stiffness is achieved by using heavy material. This, in turn, limits the speed of operation of the robot manipulation, increases sizes of actuators, boosts energy consumption and increases the overall cost. Moreover, the payload to robot weight ratio, under such situations, is low. Conversely, flexible robot manipulators exhibit many advantages over rigid robots: they require less material, are lighter in weight, consume less power; require smaller actuators; are more manoeuvrable and transportable, have less overall cost and higher payload to robot weight ratio (Book and Majette, 1983).

However, control of flexible manipulators to maintain accurate position is an extremely important problem. Due to the flexible nature of the system, the dynamics are highly non-linear and complex. Problems arise due to lack of sensing, vibration due to system flexibility and incapability of precise positioning because of the flexible nature of the system and the difficulty to obtain an accurate model (Piedboeuf *et al.*, 1993; Yurkovich, 1992). Therefore, flexible manipulators have not been favoured in production industries, as the manipulator is required to have a reasonable end-point accuracy in response to input commands. In this respect, a control mechanism that accounts for both rigid body and flexural motions of the system is required. If the advantages associated with lightness are not to be sacrificed, accurate models and efficient controllers have to be developed.

Various approaches have previously been developed for modelling of flexible manipulators (Azad, 1995). These can be divided into two categories. The first approach looks at obtaining approximate modes by solving the partial differential equation (PDE) characterising the dynamic behaviour of a flexible manipulator system. Previous investigations utilising this approach for a single-link flexible manipulator have shown that the model eigenvalues agree well with experimentally determined frequencies of the vibratory model (Book, 1984; Cannon and Schmitz, 1984; Hasting and Book, 1987). However, using this approach, such a model does not always represent the fine details of the system (Hughes, 1987).

The second approach uses numerical analysis methods based on finite difference (FD) and finite element (FE) methods to solve the PDE. Previous simulation studies using FD methods have shown that the method is simple in mathematical terms and is more appropriate

in applications involving uniform structures such as flexible manipulator systems. Further studies have shown the relative simplicity of the method (Kourmoulis, 1990). This approach has previously been utilised in obtaining the dynamic characterisation of single-link flexible manipulator systems incorporating damping, hub inertia and payload (Tokhi and Azad, 1995; Tokhi *et al.*, 1995). Experiments have also been conducted, which have shown that an acceptable agreement between simulation and experimental results is obtained.

The FE method has been successfully used to solve many material and structural problems. The method involves discretising the actual system into a number of elements with associated elastic and inertia properties of the system. This gives approximate static and dynamic characterisation of the actual system (Rao, 1989). The performance of this technique in modelling of flexible manipulators has also been investigated (Menq and Chen, 1988; Tokhi and Mohamed, 1999; Tokhi *et al.*, 1997; Usoro *et al.*, 1986). These investigations have shown that the method can be used to obtain a good representation of the system. Moreover, the FE method exhibits several advantages over the FD method (Tokhi *et al.*, 1997). However, most of the investigations utilising the FE method have not been supported by experiments. Moreover, the effect of damping has not been adequately addressed in the FE modelling process of the manipulator. The damping in the real system is expected to make the residual motions to converge to zero, as the energy is dissipated, and not to change the resonance modes of the system (Poerwanto, 1998).

This paper presents theoretical and experimental investigations into the dynamic characterisation of a single-link flexible manipulator system. A dynamic model of the system is developed using the finite element method, incorporating structural damping. The simulation algorithm thus developed is implemented in Matlab. The performance and accuracy of the modelling approach is assessed in comparison to a laboratory scale experimental flexible manipulator. To study the effect of number of elements, the results are evaluated with increasing number of elements in the algorithm. Theoretically, more accurate results will be obtained with increasing number of elements, but at the expense of higher execution times. Experimental results are presented for validation of the developed modelling approach. The experiments were conducted using a flexible manipulator experimental-rig. Simulation and experimental results are compared and analysed in both the time and frequency domains to assess the accuracy of the model in representing the actual system. The work presented forms the basis of design and development of suitable control strategies for flexible manipulator systems.

2. The Flexible Manipulator System

This section describes the flexible manipulator system used in this study. Several assumptions utilised in the process of obtaining the dynamic equations of motion of the system using FE methods are briefly discussed. Moreover, the main components of the flexible manipulator experimental-rig are described. A description of the single-link flexible manipulator system considered in this work, is shown in Figure 1, where **XOY** and **POQ** represent the stationary and moving co-ordinates respectively. Both axes lie in a horizontal plane and all rotation occurs about a vertical axis. $\tau(t)$ represents the applied torque at the hub, by a drive motor. E, I, ρ and A represent the Young modulus, second moment of area, mass density per unit volume and cross sectional area of the manipulator respectively. Because the beam is long and slender, transverse shear and rotary inertia effects are neglected. This allows the use of Bernoulli-Euler beam theory to model the elastic behaviour of the manipulator. The manipulator is assumed to be stiff in vertical bending and torsion, thus allowing it to vibrate dominantly in the horizontal direction. In this work, the gravity effects are neglected as the manipulator movement is confined to the **XOY** plane. Moreover, the beam is considered to have constant cross section and uniform material properties throughout.

The experimental-rig used in this work consists of three main parts: a flexible arm, measuring devices and a processor. Figure 2 shows the schematic diagram of the experimental-rig. The flexible arm is constructed using a piece of thin aluminium alloy with length, $L = 0.9$ m, width = 19.008 mm, thickness = 3.2004 mm, $E = 71\times10^9$ N/m^2, I =5.1924 m^4 and ρ = 2710 kg/m^3. The test-rig is equipped with U9M4AT type printed circuit motor at the hub driving the flexible manipulator. The motor is chosen as the drive actuator due to its low inertia, low inductance and physical structure (PMI Motion Technologies, 1988). In this work, a linear drive amplifier LA5600 manufactured by Electro-Craft Corporation is used as a motor driver (Electrocraft Corporation, 1985). The motor drive amplifier produces a current proportional to the input voltage.

The measuring devices used in this work are the shaft encoder, tachometer and an accelerometer along the arm. The shaft encoder, with a resolution of 2048 pulses, was used to measure the hub angle of the manipulator. A precision interface circuit consisting of a TCHT2000 incremental encoder interface chip and MP7636A double buffered 16 bit multiplexing digital to analogue (D/A) converter was then developed to convert the shaft encoder output to an analogue signal. On the other hand, the tachometer is used for

measurement of the hub velocity. A miniature integrated circuit piezoelectric accelerometer 303A03 is located at the end-point of the flexible arm to measure the end-point acceleration. The accelerometer has a built-in FET source follower which lowers the output impedance level. The low impedance output allows the use of long cables without an appreciable signal loss or distortion.

The processor used for this experimental-rig is an IBM-PC compatible based on 486DX2 50 MHz. Data acquisition and control are accomplished through the utilisation of RTI-815 I/O board. This board can provide a direct interface between the processor, actuator and sensors. The experimental set-up requires one analogue output to the motor driver amplifier and four analogue inputs from the hub angle, hub velocity, end-point acceleration and motor current sensor. The interface board is used with a conversion speed of 25 μ sec for A/D conversion and settling time of 20 μ sec for D/A conversion, which are adequate for the system under consideration.

3. Algorithm Development

This section focuses on the development of the simulation algorithm characterising the dynamic behaviour of the flexible manipulator system using FE methods. Firstly, the method is briefly discussed. Then formulations to obtain the mass, stiffness and damping matrices and the dynamic equations of motion of the manipulator, utilising the Lagrange equation, are presented. The equation of motion is expressed in state-space form, so that it can be solved using control system approaches.

3.1 The Finite Element Method

Since its introduction in the 1950s, the FE method has been continually developed and improved (Rao, 1989). The FE method involves decomposing a structure into several simple pieces or elements. The elements are assumed to be interconnected at certain points, known as nodes. For each element, an equation describing the behaviour of the element is obtained through an approximation technique. The elemental equations are then assembled together to form the system equation. It is found that by reducing the element size of the structure, that is, increasing the number of elements, the overall solution of the system equation can be made to converge to the exact solution.

The main steps in an FE analysis include (1) discretisation of the structure into elements; (2) selection of an approximating function to interpolate the result; (3) derivation of the basic element equation; (4) calculation of the system equation; (5) incorporation of the boundary conditions and (6) solving the system equation with the inclusion of the boundary conditions. In this manner, the flexible manipulator is treated as an assemblage of n elements and the development of the algorithm can be divided into three main parts: the FE analysis, state-space representation and obtaining and analysing the system transfer function.

3.2 *Simulation Algorithm*

For an angular displacement $\theta(t)$ and an elastic deflection $w(x,t)$, the total displacement $y(x,t)$ of a point along the manipulator at a distance x from the hub can be described as a function of both the rigid body motion $\theta(t)$ and elastic deflection $w(x,t)$ measured from the line OX as

$$y(x,t) = x\theta(t) + w(x,t) \tag{1}$$

and velocity $v(x,t)$ of any point can be obtained as

$$v(x,t) = \frac{\partial y(x,t)}{\partial t} = x\frac{\partial \theta(t)}{\partial t} + \frac{\partial w(x,t)}{\partial t}$$

Using the standard FE method to solve dynamic problems, leads to the well-known equation

$$w(x,t) = N_a(x)\,Q_a(t) \tag{2}$$

where $N_a(x)$ and $Q_a(t)$ represent the shape function and nodal displacement respectively. For the flexible manipulator under consideration, $w(x,t)$ in equation (2) represents the residual motion. The manipulator is divided into n elements. As a consequence of using the Bernoulli-Euler beam theory, the finite element method requires each node to possess two degrees of freedom, a transverse deflection and rotation. These necessitate the use of Hermite cubic basis functions as the element shape function (Ross, 1996). Hence, for the elemental length l, the shape function can be obtained as

$$N_a(x) = \begin{bmatrix}\phi_1(x) & \phi_2(x) & \phi_3(x) & \phi_4(x)\end{bmatrix}$$

where

$$\phi_1(x) = 1 - \frac{3x^2}{l^2} + \frac{2x^3}{l^3} \; ; \; \phi_2(x) = x - \frac{2x^2}{l} + \frac{x^3}{l^2} \quad \text{and}$$

$$\phi_3(x) = \frac{3x^2}{l^2} - \frac{2x^3}{l^3} \; ; \; \phi_4(x) = \frac{x^3}{l^2} - \frac{x^2}{l}$$

For element n the nodal displacement vector is given as

$$Q_a(t) = \begin{bmatrix} w_{n-1}(t) & \theta_{n-1}(t) & w_n(t) & \theta_n(t) \end{bmatrix}$$

where $w_{n-1}(t)$ and $w_n(t)$ are the elastic deflections of the element and $\theta_{n-1}(t)$ and $\theta_n(t)$ are the corresponding angular displacements. Substituting for $w(x,t)$ from equation (2) into equation (1) and simplifying yields

$$y(x,t) = N(x)\, Q(t) \tag{3}$$

where

$$N(x) = \begin{bmatrix} x & N_a(x) \end{bmatrix} \quad \text{and} \quad Q(t) = \begin{bmatrix} \theta(t) & Q_a(t) \end{bmatrix}^T$$

The new shape function $N(x)$ and nodal displacement vector $Q(t)$ in equation (3) incorporate local and global variables. Among these, the angle $\theta(t)$ and the distance x are global variables while $N_a(x)$ and $Q_a(t)$ are local variables. Defining $s = x - \sum_{i=1}^{n-1} l_i$ as a local variable of the nth element, where l_i is the length of the ith element, the kinetic energy of an element 'e' can be expressed as

$$T_e = \int_0^l \rho A \left[\frac{\partial y(s,t)}{\partial t} \right]^2 ds = \frac{1}{2} \int_0^l \rho A \dot{Y}^T \dot{Y}\, ds = \frac{1}{2} \dot{Q}^T \left[\int_0^l \rho A (N^T N)\, ds \right] \dot{Q} \tag{4}$$

and potential energy of the element can be obtained as

$$P_e = \frac{1}{2} \int_0^l EI \left[\frac{\partial^2 y(s,t)}{\partial s^2} \right]^2 ds = \frac{1}{2} \int_0^l EI\, (BQ)^T (BQ)\, ds = \frac{1}{2} Q^T \left[\int_0^l EI\, (B^T B)\, ds \right] Q \tag{5}$$

where $B = \dfrac{d^2 N}{ds^2}$.

Defining M_e and K_e as

$$M_e = \int_0^l \rho A (N^T N)\, ds = \text{element mass matrix} \tag{6}$$

$$K_e = \int_0^l EI\,(B^T B)\,ds \;= \text{element stiffness matrix} \tag{7}$$

and solving equations (6) and (7) for the n elements, the element mass and stiffness matrices can be obtained as

$$M_n = \frac{\rho A l}{420}\begin{bmatrix} m_{11} & m_{12} & m_{13} & m_{14} & m_{15} \\ m_{21} & 156 & 22l & 54 & -13l \\ m_{31} & 22l & 4l^2 & 13l & -3l^2 \\ m_{41} & 54 & 13l & 156 & -22l \\ m_{51} & -13l & -3l^2 & -22l & 4l^2 \end{bmatrix}$$

$$K_n = \frac{EI}{l^3}\begin{bmatrix} 0 & 0 & 0 & 0 & 0 \\ 0 & 12 & 6l & -12 & 6l \\ 0 & 6l & 4l^2 & -6l & 2l^2 \\ 0 & -12 & -6l & 12 & -6l \\ 0 & 6l & 2l^2 & -6l & 4l^2 \end{bmatrix}$$

where

$$\begin{aligned} m_{11} &= 140l^2(3n^2 - 3n + 1) \\ m_{12} &= m_{21} = 21l(10n - 7) \\ m_{13} &= m_{31} = 7l^2(5n - 3) \\ m_{14} &= m_{41} = 21l(10n - 3) \\ m_{15} &= m_{51} = -7l^2(5n - 2) \end{aligned}$$

Assembling the element mass and stiffness matrices, the total kinetic and potential energies from equations (4) and (5) can be written as

$$T = \frac{1}{2}\dot{Q}^T M \dot{Q}$$

$$P = \frac{1}{2}Q^T K Q$$

where $M = \sum_{e=1}^{n} M_e$ is a global mass matrix and $P = \sum_{e=1}^{n} P_e$ is a global stiffness matrix of the manipulator. The dynamic equations of motion of the flexible manipulator can be derived utilising the Lagrange equation;

$$\frac{d}{dt}\left\{\frac{\partial L}{\partial \dot{Q}}\right\} - \left\{\frac{\partial L}{\partial Q}\right\} = F$$

where $L = T - P$ is the Lagrangian and F is a vector of external forces. Considering the damping, the desired dynamic equations of motion of the system can be obtained as

$$M\ddot{Q}(t) + D\dot{Q}(t) + KQ(t) = F(t) \tag{8}$$

where $F(t)$ is the vector of applied forces and torque, $Q(t) = [\theta \quad w_0 \quad \theta_0 \quad . \quad . \quad . \quad w_n \quad \theta_n]^T$ and D is a global damping matrix, normally determined through experimentation. The damping ratio typically ranges from 0.007 to 0.01 (Hasting and Book, 1987).

For the flexible manipulator under consideration, the global mass matrix can be represented as

$$M = \begin{bmatrix} M_{\theta\theta} & M_{\theta w} \\ M_{\theta w} & M_{ww} \end{bmatrix}$$

where M_{ww} is associated with the elastic degrees of freedom (residual motion), $M_{\theta w}$ represents the coupling between these elastic degrees of freedom and the hub angle θ and $M_{\theta\theta}$ is associated with the inertia of the system about the motor axis. Similarly, the global stiffness matrix can be written as

$$K = \begin{bmatrix} 0 & 0 \\ 0 & K_{ww} \end{bmatrix}$$

where K_{ww} is associated with the elastic degrees of freedom (residual motion). It can be shown that the elastic degrees of freedom do not couple with the hub angle through the stiffness matrix.

The global damping matrix D in equation (8) can be represented as

$$D = \begin{bmatrix} 0 & 0 \\ 0 & D_{ww} \end{bmatrix}$$

where D_{ww} denotes the sub-matrix associated with the material damping. The matrix is obtained by assuming that the beam exhibits the characteristics of Rayleigh damping. This proportional damping model has been assumed because it allows experimentally determined damping ratios of individual modes to be used directly in forming the global matrix. It also allows assignment of individual damping ratios to individual modes, such that the total beam damping is the sum of the damping in the modes (Chapnik *et al.*, 1991). Using this assumption, the damping can be obtained as

$$D_{ww} = \alpha M_{ww} + \beta K_{ww} \tag{9}$$

where

$$\alpha = \frac{2 f_1 f_2 (\xi_1 f_2 - \xi_2 f_1)}{f_2^2 - f_1^2} \; ; \; \beta = \frac{2 (\xi_2 f_2 - \xi_1 f_1)}{f_2^2 - f_1^2};$$

with ξ_1 , ξ_2, f_1 and f_2 representing the damping ratios and natural frequencies of modes 1 and 2 respectively.

The M, D and K matrices in equation (8) are of size $m \times m$ and $F(t)$ is of size $m \times 1$, where $m = 2n + 1$. For the manipulator, considered as a pinned-free arm, with the applied torque τ at the hub, the flexural and rotational displacement, velocity and acceleration are all zero at the hub at $t = 0$ and the external force is $F(t) = [\tau \quad 0 \quad \cdots \quad 0]^T$. Moreover, in this work, it is assumed that $Q(0) = 0$. The matrix differential equation in equation (8) can be represented in a state-space form as

$$\dot{v} = Av + Bu$$
$$y = Cv$$

where

$$\mathbf{A} = \left[\begin{array}{c|c} 0_m & I_m \\ \hline -M^{-1}K & -M^{-1}D \end{array}\right], \quad \mathbf{B} = \left[\begin{array}{c} 0_{m\times 1} \\ \hline M^{-1} \end{array}\right],$$

$$\mathbf{C} = [0_m \; | \; I_m], \qquad \mathbf{D} = [0_{2m\times 1}]$$

0_m is an $m \times m$ null matrix, I_m is an $m \times m$ identity matrix, $0_{m\times 1}$ is an $m \times 1$ null vector,

$$u = [\tau \quad 0 \quad \cdots \quad 0]^T, \; v = \left[\theta \quad w_1 \quad \theta_1 \quad \cdots \quad w_n \quad \theta_n \quad \dot{\theta} \quad \dot{w}_1 \quad \dot{\theta}_1 \quad \cdots \quad \dot{w}_n \quad \dot{\theta}_n\right]^T$$

Solving the state-space matrices gives the vector of states v, that is, the angular, nodal flexural and rotational displacements and velocities.

4. Results

In this section, a set of simulation and experimental results of the dynamic behaviour of the flexible manipulator system are presented in the time and frequency domains. In this work, a bang-bang signal of amplitude 0.3 Nm, shown in Figure 3, was used as an input torque applied at the hub of the manipulator. A bang-bang torque has a positive (acceleration) and negative (deceleration) period allowing the manipulator to, initially, accelerate and then decelerate and eventually stop at a target location. System responses were monitored for a duration of 3 sec with sampling time of 4 msec.

4.1 Simulation Results

The developed finite element model was implemented within the Matlab environment on a Pentium II 333MHz processor. To demonstrate the effects of damping on the system response, investigations with and without damping were carried out. In this work, the damping ratios were assumed as 0.007 and 0.01 for vibration modes 1 and 2 respectively. Using 12 Hz and 35 Hz as the first two resonance frequencies (Azad, 1995), α and β in equation (9) can be obtained as 0.3175 and 1.2980 respectively. To investigate the accuracy of the FE simulation algorithm in characterising the behaviour of the flexible manipulator, the algorithm was implemented on the basis of varying the number of elements from 1 to 20.

Figures 4 and 5 show the end-point displacement, hub-angle, hub-velocity, residual motion, end-point acceleration and spectral density of hub-angle of the manipulator without the presence of damping using 1 and 10 elements respectively. It is noted that steady-state levels of end-point displacement and hub angle of 0.6 m and 38° respectively were achieved within 0.9 sec using one or more elements. These proved that a satisfactory dynamic behaviour of a flexible manipulator, up to the second mode, could be achieved with one element. Further modes of the system are obtained with increasing the number of elements. As expected, without the damping effect, the system response exhibits persistent oscillation. The results also show that the system characterises a non-minimum phase behaviour as evident from the slight undershoot that occurs at start of end-point response of the system. This agrees, as a non-collocated system, with previously developed models (Cannon and Schmitz, 1984). Using one element, the system poles and zeros were obtained as 0, 0, $\pm 90.82j$, $\pm 300.07j$ and ± 58.59, ± 229.14 respectively. The residual motion of the system is found to be characterised by the first two modes of vibration. Resonance frequencies of the system were obtained by transforming the time domain representation of the system into the frequency domain using FFT analysis. With one element, the resonance frequencies of the system were obtained as 14.49 Hz and 47.70 Hz whereas with ten elements these were as 11.99 Hz, 35.22 Hz and 65.2 Hz.

Figures 6 and 7 show the dynamic behaviour of the system in the presence of damping with 1 and 10 elements respectively. It is noted that the damping has not affected the resonance frequencies of the system, but has resulted in considerable attenuation in the system response amplitude. Analysing the system time response, it is noted that the hub-velocity, end-point acceleration and end-point residual motion of the system converged to zero within 1.8

sec. It is also evidenced from the spectral densities of the system response, that the damping has not affected the resonance frequencies of vibration of the system. However, with damping, the level of vibration reduces as expected. By increasing the number of elements, the system resonance frequencies converge to more accurate values, but, at the expense of higher execution times. This is mainly due to an increase in the size of the mass, damping, stiffness and state-space matrices. The inter-relation between the number of elements, execution time and resonance frequencies of the system is summarised in Table 1.

4.2 Experimental Results

Experiments using the experimental-rig were conducted for validation of the developed FE model. In the experiments, the hub-angle, hub-velocity and end-point acceleration were measured and the corresponding spectral densities were obtained. These were then compared with the simulation results. Figure 8 shows the hub-angle, hub-velocity, end-point acceleration, with their spectral densities, of the flexible manipulator. It is noted that for the hub-angle, the steady-state level of 38° was achieved within 1.8 sec. The first three modes of vibration were obtained as 11.72 Hz, 35.15 Hz and 65.60 Hz.

4.3 Model Validation

Validation of a dynamic model for use in simulation and control is an important step before the model can be employed with confidence. Typically, model validation can be considered in two parts: frequency-domain validation, which involves the resonance frequencies of the system, and time-domain validation, which focuses on the time response of various system states to an input command. Matching of natural frequencies is a good indication of accurately modelled mass and stiffness properties. Time domain results show the effects of assumptions concerning the non-linear terms in the equations of motion.

Validation of the developed finite element model was carried out by comparing simulation and experimental results in time and frequency domains. Comparisons of Figures 6, 7 and 8, show that a close agreement between experimental and simulation results in the time responses and resonance frequencies was obtained. For the hub-angle, a steady-state level of 38° was achieved within 1.8 sec in both cases. Similar characteristics are also noted in the transient response of the system. Furthermore, reasonably close agreement between the simulation and experimental results is noted with the hub-velocity and end-point acceleration

responses. It is also noted in Table 1 that the first three modes of vibration of the system converged to 11.99 Hz, 35.22 Hz and 65.20 Hz with 10 elements or more. The experimental results, however, gave 11.72 Hz, 35.15 Hz and 65.60 Hz. The corresponding errors between the simulation and experimental results for modes 1, 2 and 3 are accordingly 2.3 %, 0.2 % and 3.9 % respectively, which are considered negligibly small. It can thus be concluded that FE methods can successfully be used for modelling of a flexible manipulator. Moreover, these validate the assumptions used in this work.

5. Conclusion

Theoretical and experimental investigations into the dynamic characterisation of a single-link flexible manipulator system have been presented. A dynamic model of the manipulator has been developed using FE methods. The performance and accuracy of the algorithm has been studied in comparison to an experimental-rig. Moreover, effects of damping on the system have been addressed. Experiments have been performed using the experimental-rig and used for validation of the FE model. Comparisons of simulation and experimental results have demonstrated a satisfactory and close agreement between the simulated and experimental time responses and resonance frequencies of the system.

6. References

AZAD, A.K.M. (1995). *Analysis and design of control mechanisms for flexible manipulator systems*, PhD. Thesis, Department of Automatic Control and Systems Engineering, University of Sheffield, UK.

BOOK, W.J. (1984). Recursive lagrangian dynamics of flexible manipulator arms, *International Journal of Robotics Research,* **3**(3), pp. 87-101.

BOOK, W.J. and MAJETTE, M. (1983). Controller design for flexible distributed parameter mechanical arm via combined state-space and frequency domain technique, *Transactions of ASME: Journal of Dynamic Systems, Measurement and Control*, **105**(4), pp. 245-254.

CANNON, R.H. and SCHMITZ, E. (1984). Initial experiment on the end-point control of a flexible one-link robot, *International Journal of Robotics Research*, **3**(3), pp. 62-75.

CHAPNIK, B.V., HEPPLER, G.R. and APLEVICH, J.D. (1991). Modeling impact on a one-link flexible robotic arm, *IEEE Transactions on Robotics and Automation*, **7**(4), pp. 479-488.

ELECTROCRAFT CORPORATION. (1985). *DC motors speed control servo systems*, Electrocraft Corporation / Robbins & Mayers, Minnesota.

HASTING, G.G. and BOOK, W.J. (1987). A linear dynamic model for flexible robot manipulators, *IEEE Control Systems Magazine*, **7**, pp. 61-64.

HUGHES, P.C. (1987). Space structure vibration modes: How many exist? Which are important, *IEEE Control Systems Magazine*, **7**, pp. 22-28.

KOURMOULIS, P.K. (1990). *Parallel processing in the simulation and control of flexible beam structures*, PhD. Thesis, Department of Automatic Control and Systems Engineering, The University of Sheffield, UK.

MENQ, C.H. and CHEN, J.-S. (1988). Dynamic modeling and payload-adaptive control of a flexible manipulator, *Proceedings. of IEEE International Conference on Robotics and Automation*, Philadelphia, pp. 488-493.

PIEDBOEUF, J.-C., FAROOQ, M., BAYOUMI, M.M., LABINAZ, G. and ARGOUN, M.B. (1993). Modelling and Control of flexible manipulators – Revisited, *Proceedings of 36th Midwest Symposium on Circuits and Systems*, Detroit, pp. 1480-1483.

PMI MOTION TECHNOLOGIES. (1988). *General application of printed motors*, PMI Motion Technologies, New York.

POERWANTO, H. (1998). *Dynamic simulation and control of flexible manipulator systems*, PhD. Thesis, Department of Automatic Control and Systems Engineering, University of Sheffield, UK.

RAO, S.S. (1989). *The finite element method in engineering*, Pergamon Press, Oxford.

ROSS, C.T.F. (1996). *Finite element techniques in structural mechanics*, Albion Publishing Limited, West Sussex.

TOKHI, M.O. and AZAD, A.K.M. (1995). Real time finite difference simulation of a single-link flexible manipulator incorporating hub inertia and payload, *Proceedings of IMechE-I: Journal of Systems and Control Engineering*, **209**(I1), pp. 21-33.

TOKHI, M.O. and MOHAMED, Z. (1999). Finite element approach to dynamic modelling of a flexible robot manipulator: Performance evaluation and computational requirements, *Communications in Numerical Methods in Engineering*, **15**, pp. 669-676.

TOKHI, M.O., MOHAMED, Z. and AZAD, A.K.M. (1997). Finite difference and finite element approaches to dynamic modelling of a flexible manipulator, *Proceedings of IMechE-I: Journal of Systems and Control Engineering*, **211**(I2), pp. 145-156.

TOKHI, M.O., POERWANTO, H. and AZAD, A.K.M. (1995). Dynamic simulation of flexible manipulator incorporating hub inertia, payload and damping, *Machine Vibration*, **4**, pp. 106-124 (1995).

USORO, P.B., NADIRA, R. and MAHIL, S.S. (1986). A finite element/lagrange approach to modelling lightweight flexible manipulators" *Transactions of ASME: Journal of Dynamic Systems, Measurement and Control*, **108**, pp. 198-205.

YURKOVICH, S. (1992). Flexibility effects on performance and control, *Robot Control*, IEEE Press, Part 8, pp. 321-323.

TABLES

Table 1: Relation between the number of elements, execution times and resonance frequencies of the flexible manipulator.

Number of elements	Execution time (sec)	Resonance frequencies (Hz)		
		Mode 1	Mode 2	Mode 3
1	0.38	14.49	47.7	-
2	0.44	11.99	35.71	77.17
3	0.55	11.99	35.46	65.68
5	0.67	11.99	35.46	65.43
10	0.98	11.99	35.22	65.2
20	2.72	11.99	35.22	65.2

FIGURES

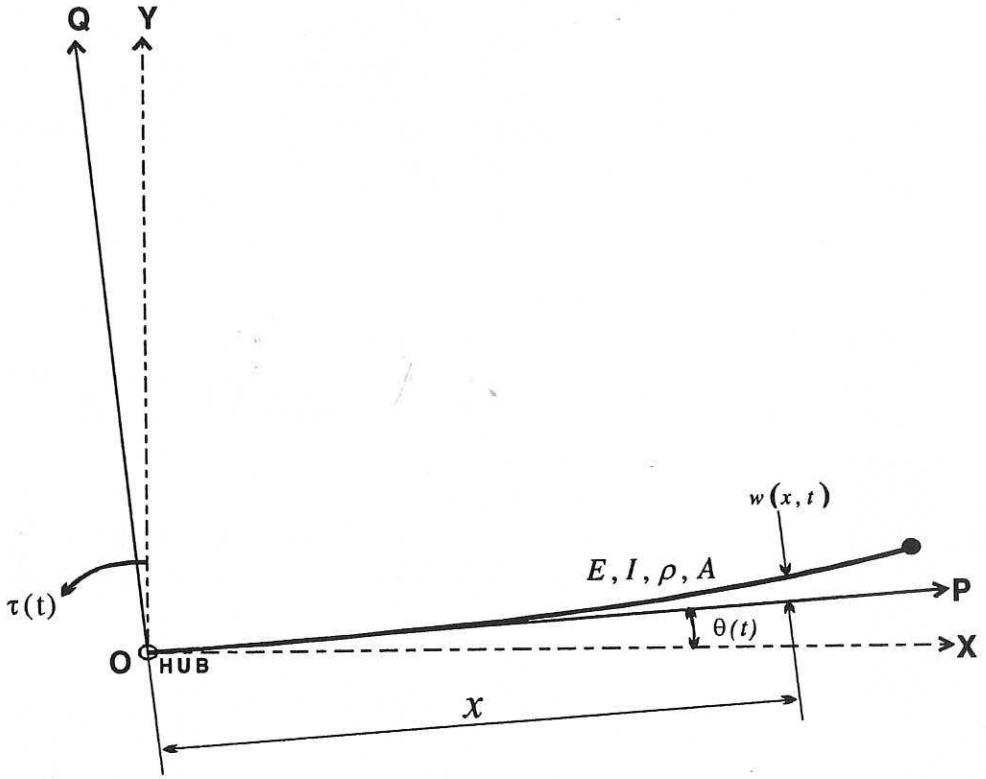

Figure 1: Description of the flexible manipulator system.

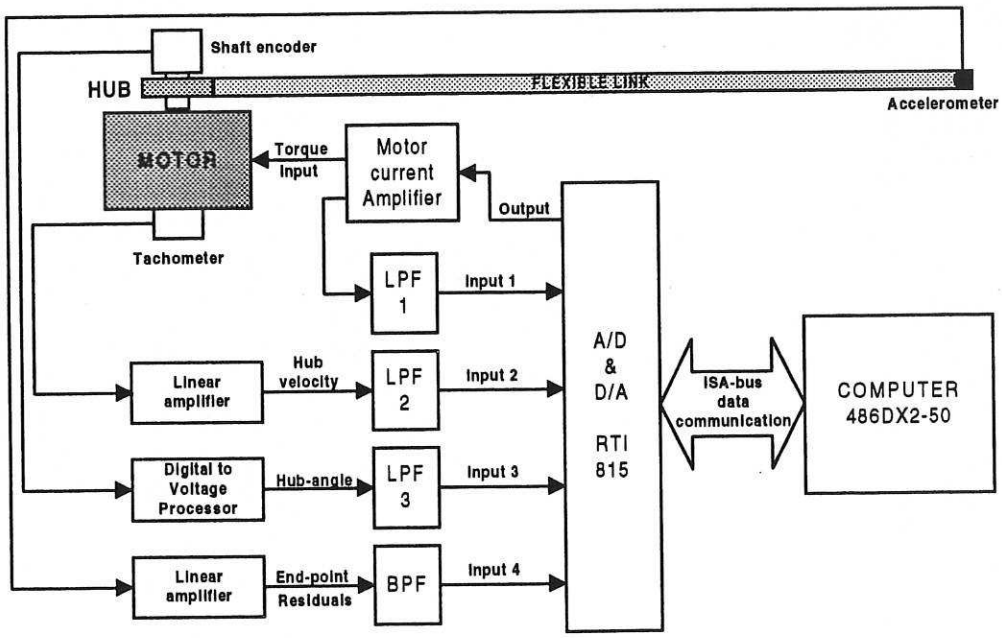

Figure 2: Schematic diagram of the experimental-rig.

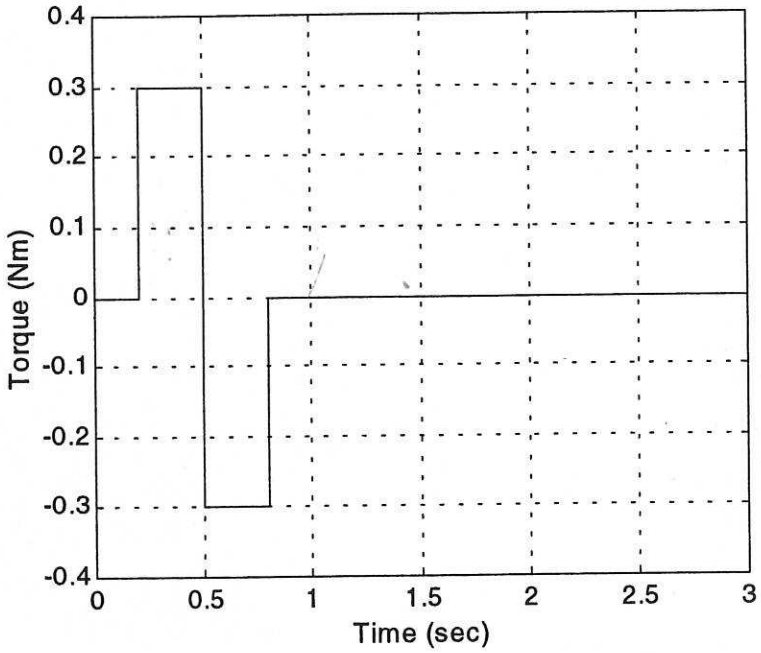

Figure 3: The bang-bang input torque.

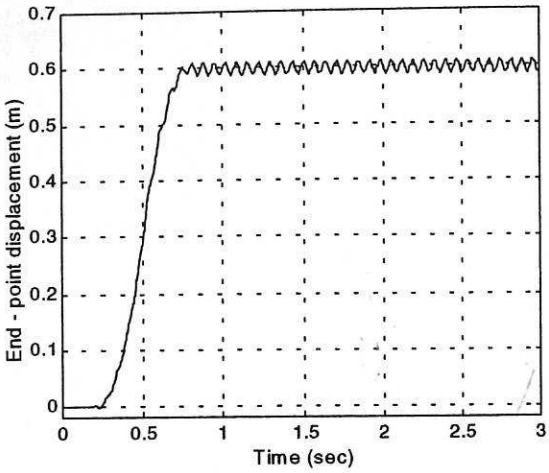

(a) End-point displacement.

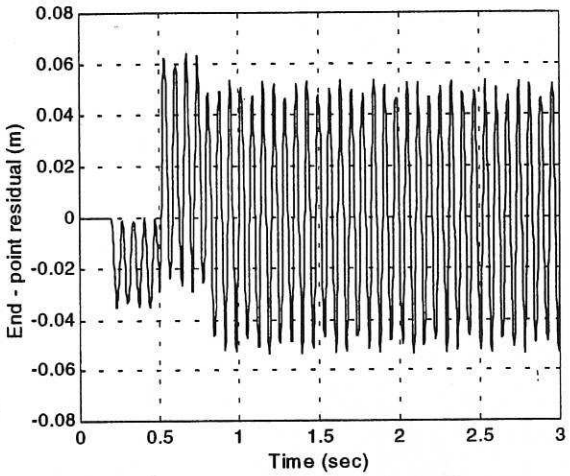

(b) End-point residual motion.

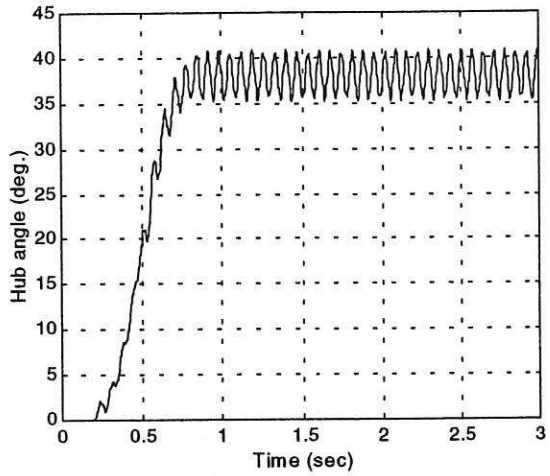

(c) Hub-angle.

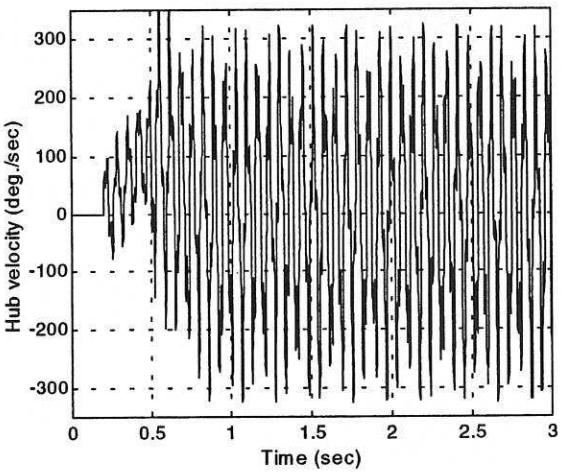

(d) Hub-velocity.

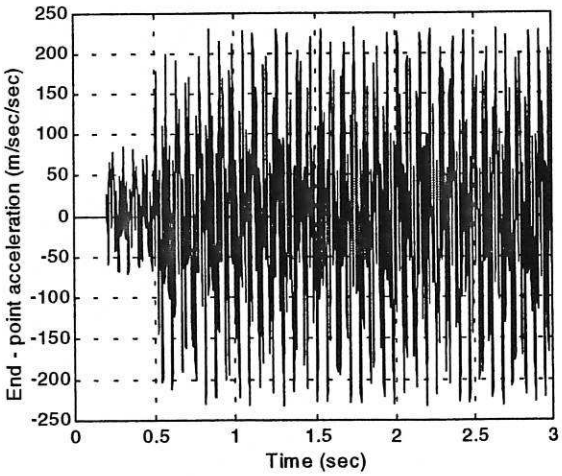

(e) End-point acceleration.

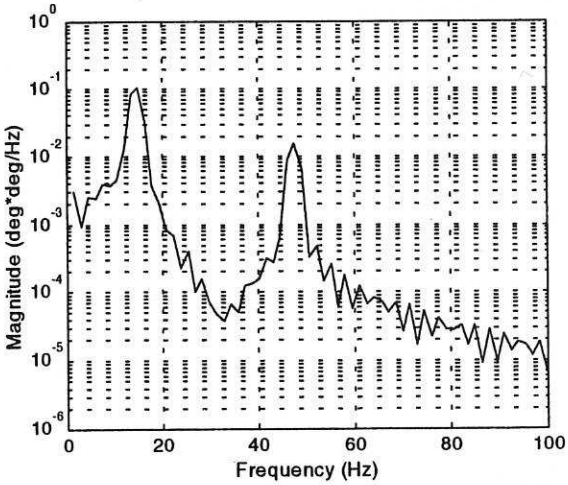

(f) Spectral density of hub-angle.

Figure 4: Simulated response of the flexible manipulator without damping; Number of elements = 1.

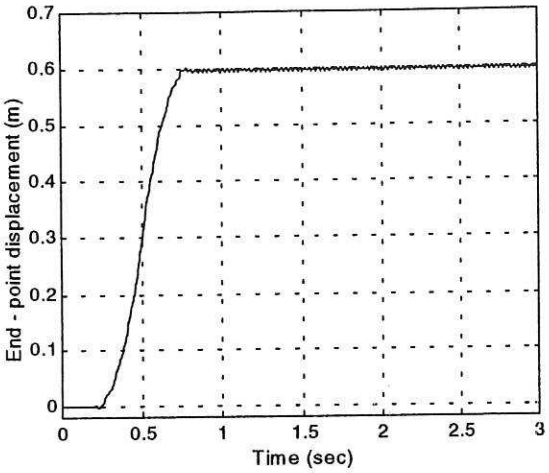

(a) End-point displacement.

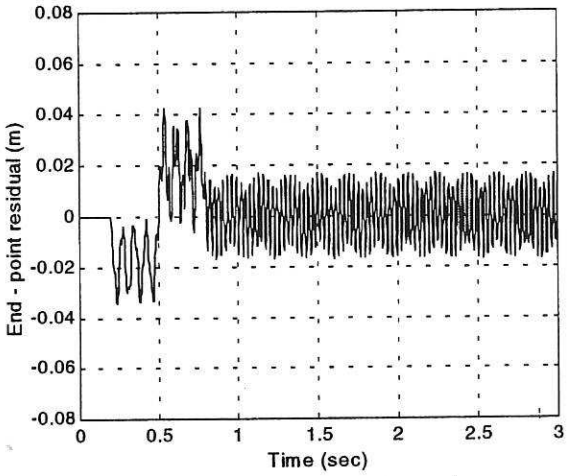

(b) End-point residual motion.

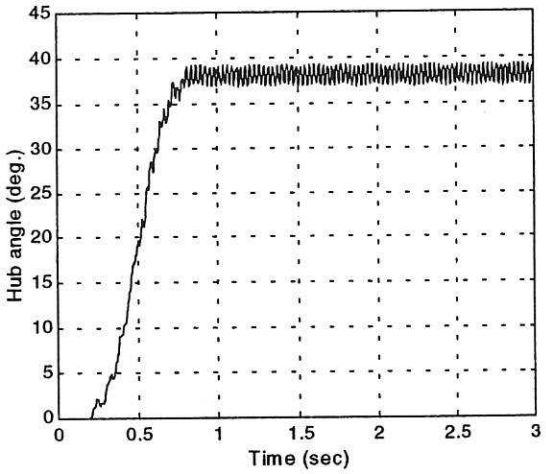

(c) Hub-angle.

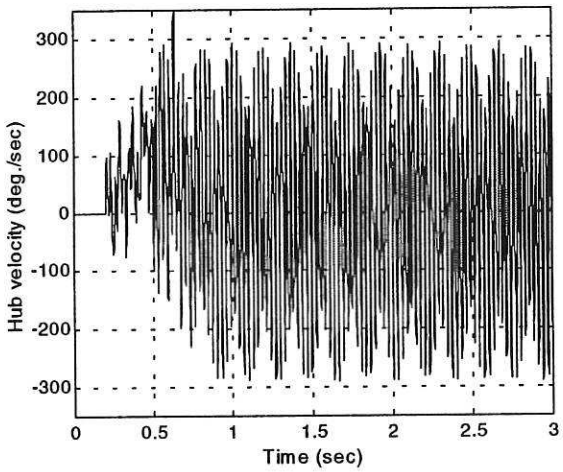

(d) Hub-velocity.

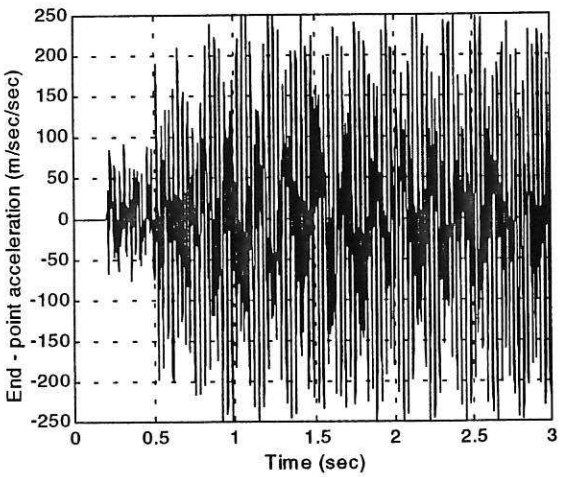

(e) End-point acceleration.

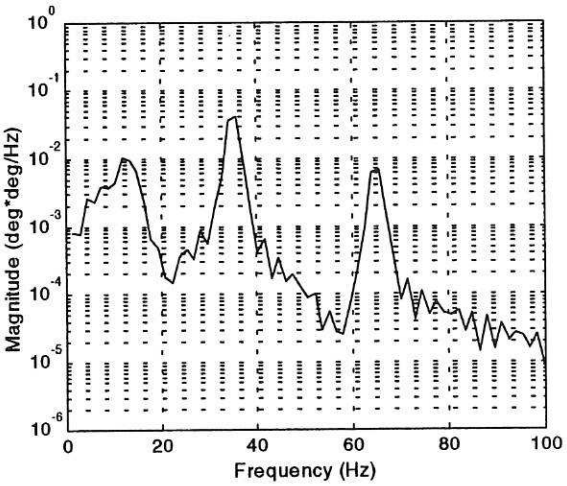

(f) Spectral density of hub-angle.

Figure 5: Simulated response of the flexible manipulator without damping; Number of elements = 10.

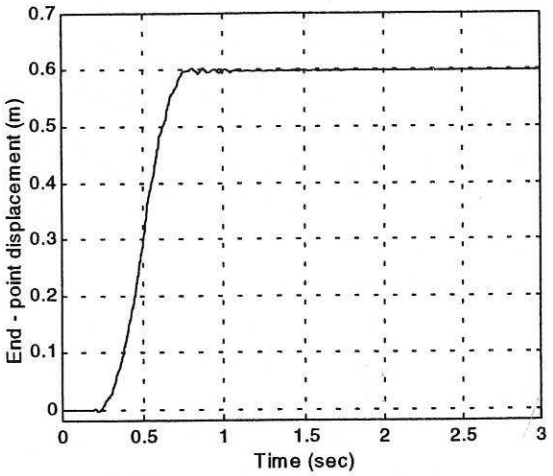

(a) End-point displacement.

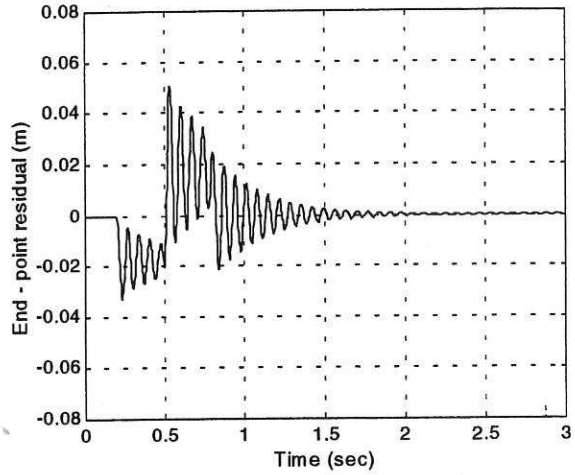

(b) End-point residual motion.

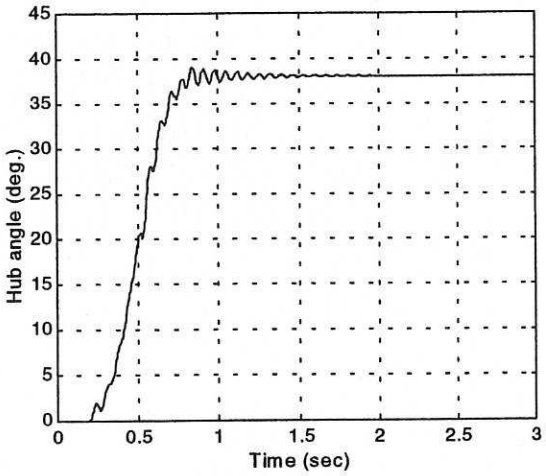

(c) Hub-angle.

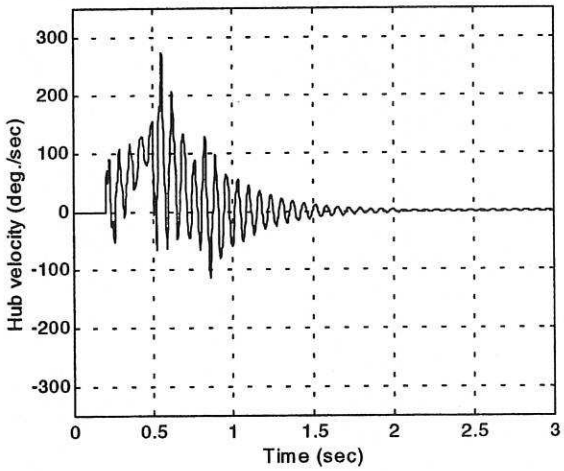

(d) Hub-velocity.

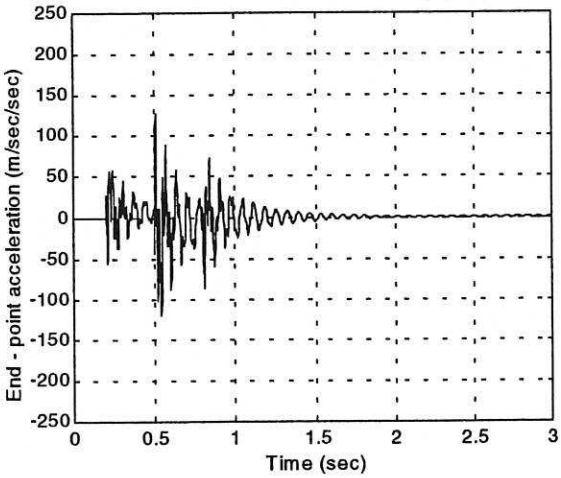

(e) End-point acceleration.

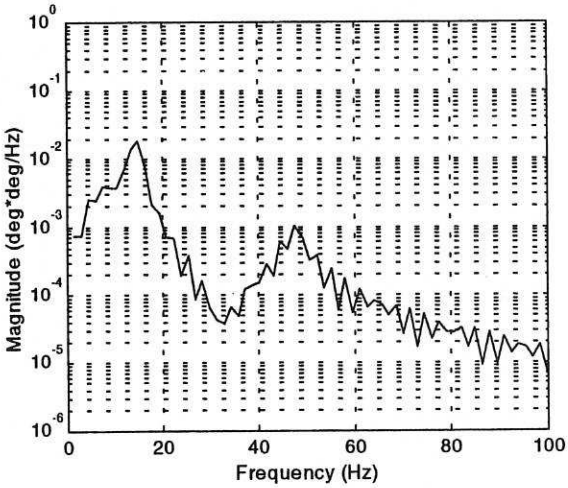

(f) Spectral density of hub-angle.

Figure 6: Simulated response of the flexible manipulator with damping; Number of elements = 1.

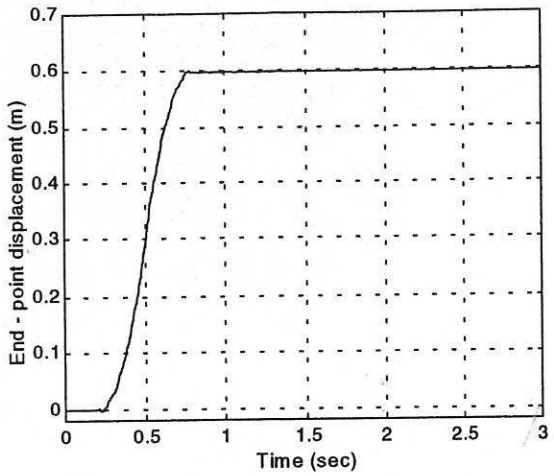

(a) End-point displacement.

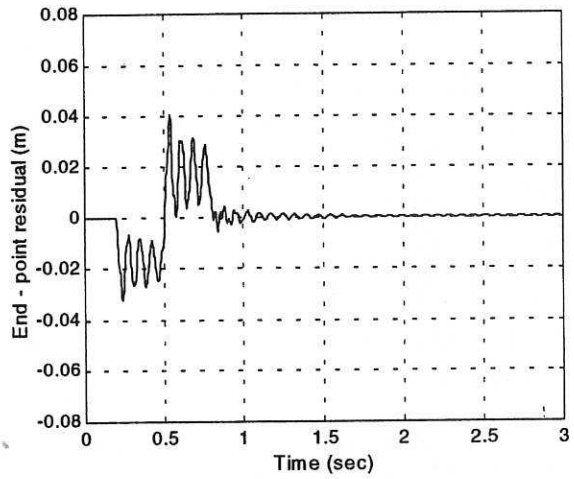

(b) End-point residual motion.

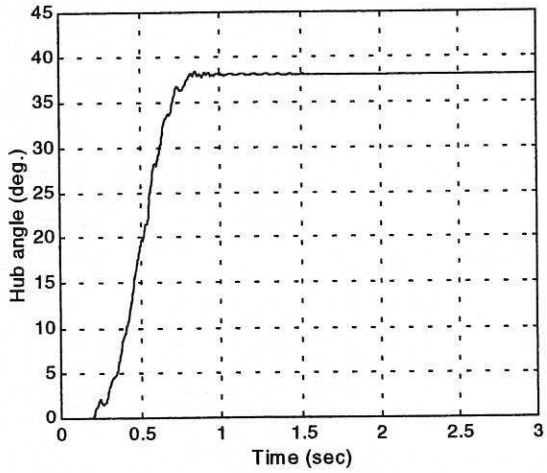

(c) Hub-angle.

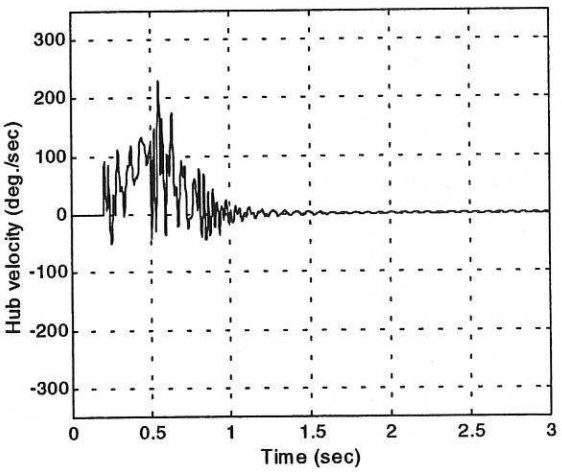

(d) Hub-velocity.

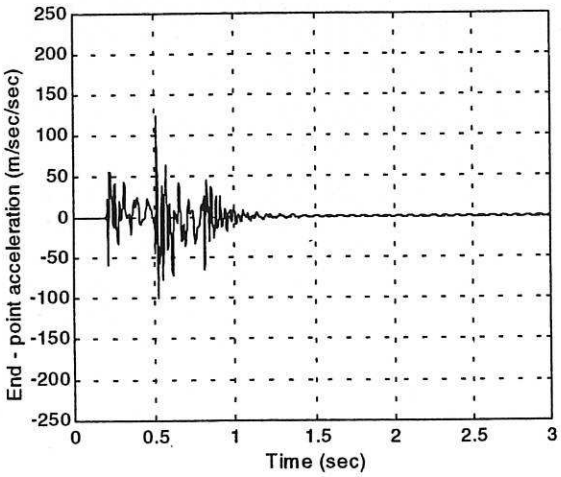

(e) End-point acceleration.

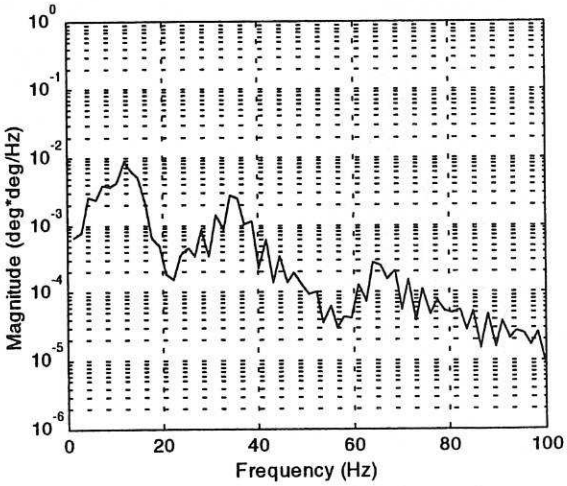

(f) Spectral density of hub-angle.

Figure 7: Simulated response of the flexible manipulator with damping; Number of elements = 10.

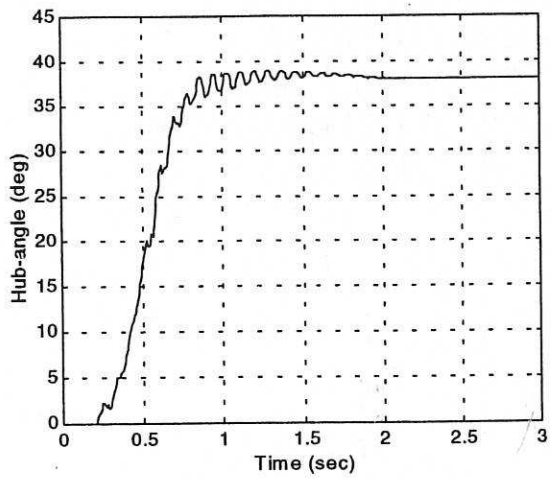

(a) Hub-angle.

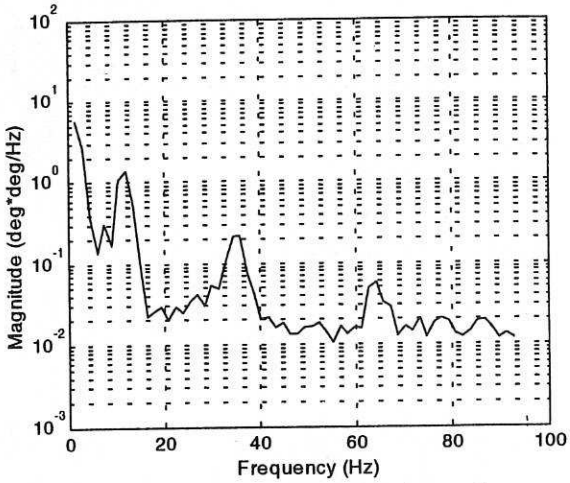

(b) Spectral density of hub-angle.

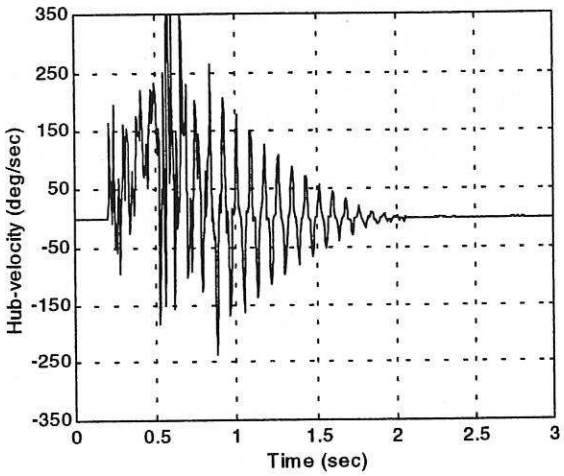

(c) Hub-velocity.

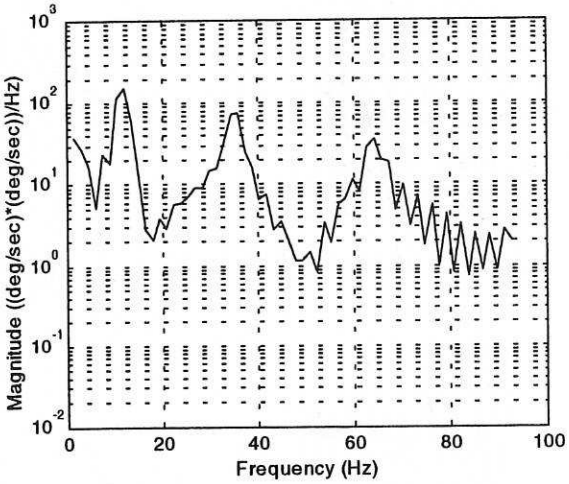

(d) Spectral density of hub-velocity.

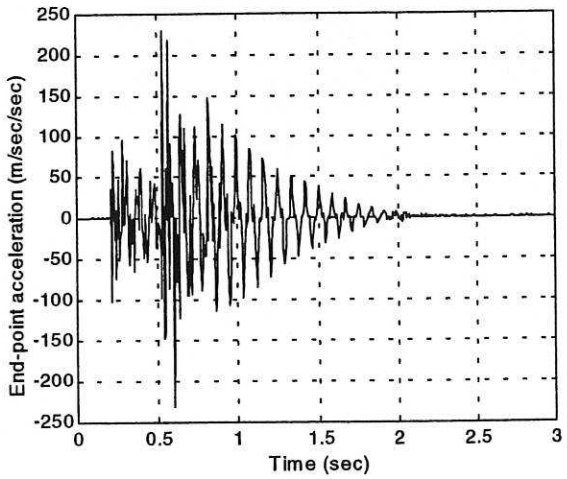

(e) End-point acceleration.

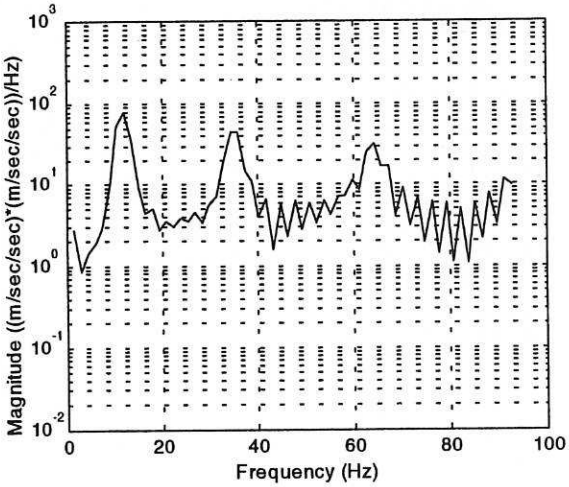

(f) Spectral density of end-point acceleration.

Figure 8: Response of the experimental flexible manipulator-rig.